NTL
49364

5

U.S. Department
of Transportation

**Federal Railroad
Administration**

# Thermomechanical Testing and Microstructural Development of Class L Steel Wheel Alloy

Office of Research and Development
Washington, DC 20590

R. M. Pelloux
D. C. Grundy

Department of Materials Science and Engineering
Massachusetts Institute of Technology
Cambridge, MA 02139

DOT/FRA/ORD-94/01
DOT-VNTSC-FRA-94-3

Final Report
March 1994

This document is available to the public through the National Technical Information Service, Springfield, VA 22161

94

**NOTICE**

This document is disseminated under the sponsorship of the Department of Transportation in the interest of information exchange. The United States Government assumes no liability for its contents or use thereof.

# REPORT DOCUMENTATION PAGE

Form Approved
OMB No. 0704-0188

Public reporting burden for this collection of information is estimated to average 1 hour per response, including the time for reviewing instructions, searching existing data sources, gathering and maintaining the data needed, and completing and reviewing the collection of information. Send comments regarding this burden estimate or any other aspect of this collection of information, including suggestions for reducing this burden, to Washington Headquarters Services, Directorate for information Operations and Reports, 1215 Jefferson Davis Highway, Suite 1204, Arlington, VA 22202-4302, and to the Office of Management and Budget, Paperwork Reduction Project (0704-0188), Washington, DC 20503.

| 1. AGENCY USE ONLY (Leave blank) | 2. REPORT DATE | 3. REPORT TYPE AND DATES COVERED |
|---|---|---|
| | March 1994 | Final Report<br>October 1992 - May 1993 |

**4. TITLE AND SUBTITLE**
Thermomechanical Testing and Microstructural Development of Class L Steel Wheel Alloy

**5. FUNDING NUMBERS**
R3026/RR328

**6. AUTHOR(S)**
R.M. Pelloux[1] and D.C. Grundy[1]

**7. PERFORMING ORGANIZATION NAME(S) AND ADDRESS(ES)**
[1]Dept. of Materials Science and Engineering*
Massachusetts Institute of Technology
Cambridge, MA 02139

Oregon Graduate Institute of Science and Technology**
Beaverton, OR 97006

**8. PERFORMING ORGANIZATION REPORT NUMBER**
DOT-VNTSC-FRA-94-3

**9. SPONSORING/MONITORING AGENCY NAME(S) AND ADDRESS(ES)**
U.S. Department of Transportation
Federal Railroad Administration
Office of Research and Development
Washington, DC 20590

**10. SPONSORING/MONITORING AGENCY REPORT NUMBER**
DOT/FRA/ORD-94/01

**11. SUPPLEMENTARY NOTES**

*under contract to:
U.S. Department of Transportation
Research and Special Programs Administration
John A. Volpe National Transportation Sys. Ctr.
Cambridge, MA 02142

**under contract to:
U.S. Department of Transportation
Federal Railroad Administration
Office of Research and Development
Washington, DC 20590

**12a. DISTRIBUTION/AVAILABILITY STATEMENT**
This document is available to the public through the National Technical Information Service, Springfield, VA 22161

**12b. DISTRIBUTION CODE**

**13. ABSTRACT (Maximum 200 words)**

Macrostructure, microstructure, and quantitative metallographic analysis is conducted on AAR Class L wheel steel specimens tested in a Gleeble 1500 under combined mechanical compression and resistance heating to temperatures above and below the austenite transformation temperature. The mechanical loading shears the as-received ferrite-pearlite microstructure. A partially or fully recrystallized microstructure is observed in the sheared regions. The recrystallized microstructure contains fine globular carbides typical of a spheroidized steel and is produced at temperatures below the austenite transformation temperature. Trends are found toward increasing recrystallized fraction with increasing temperature and decreasing fraction with increasing compression above 4.5% strain.

**14. SUBJECT TERMS**
Metallurgy; Railroad Wheels, Steel

**15. NUMBER OF PAGES**
42

**16. PRICE CODE**

| 17. SECURITY CLASSIFICATION OF REPORT | 18. SECURITY CLASSIFICATION OF THIS PAGE | 19. SECURITY CLASSIFICATION OF ABSTRACT | 20. LIMITATION OF ABSTRACT |
|---|---|---|---|
| Unclassified | Unclassified | Unclassified | |

## PREFACE

This report is the fifth of a series on the results of an engineering study of the effects of service loads on railroad vehicle wheels. The study was initiated in September 1991, in response to a request for assessment of contributing factors and corrective actions taken regarding high rates of thermal cracking in certain multiple unit powered cars used in commuter rail service.

In the first report of the series, it was noted that the material near the treads of thermally cracked wheels generally has the appearance of a spheroidized microstructure. This form is usually associated with a sequence of heating to extremely high temperatures (above 1400°F), rapid quenching to produce martensite (an extremely brittle phase), and tempering at high temperatures (800 to 900 °F) to transform the martensite to spheroidite.

Since other information had suggested that the damaged wheels were not exceeding 1200°F, even under extreme conditions, additional work was conducted to resolve the apparent inconsistency. The additional work, summarized in this report, involved laboratory tests of wheel steel samples, which were subjected to combined rapid heating and compression. The combination of heat and compression was used to simulate the environment of material near a wheel tread which is subjected to combined stop braking (heat) and rail contact (compression). The results of the laboratory tests show that the microstructure can transform at temperatures below 1200°F, if the material is also compressed, and that the transformed microstructure can have an appearance similar to that of spheroidite.

## METRIC/ENGLISH CONVERSION FACTORS

### ENGLISH TO METRIC

#### LENGTH (APPROXIMATE)

1 inch (in) = 2.5 centimeters (cm)
1 foot (ft) = 30 centimeters (cm)
1 yard (yd) = 0.9 meter (m)
1 mile (mi) = 1.6 kilometers (km)

#### AREA (APPROXIMATE)

1 square inch (sq in, $in^2$) = 6.5 square centimeters ($cm^2$)
1 square foot (sq ft, $ft^2$) = 0.09 square meter ($m_2$)
1 square yard (sq yd, $yd^2$) = 0.8 square meter ($m^2$)
1 square mile (sq mi, $mi^2$) = 2.6 square kilometers ($km^2$)
1 acre = 0.4 hectares (he) = 4,000 square meters ($m^2$)

#### MASS - WEIGHT (APPROXIMATE)

1 ounce (oz) = 28 grams (gr)
1 pound (lb) = .45 kilogram (kg)
1 short ton = 2,000 pounds (lb) = 0.9 tonne (t)

#### VOLUME (APPROXIMATE)

1 teaspoon (tsp) = 5 milliliters (ml)
1 tablespoon (tbsp) = 15 milliliters (ml)
1 fluid ounce (fl oz) = 30 milliliters (ml)
1 cup (c) = 0.24 liter (l)
1 pint (pt) = 0.47 liter (l)
1 quart (qt) = 0.96 liter (l)
1 gallon (gal) = 3.8 liters (l)
1 cubic foot (cu ft, $ft^3$) = 0.03 cubic meter ($m^3$)
1 cubic yard (cu yd, $yd^3$) = 0.76 cubic meter ($m^3$)

#### TEMPERATURE (EXACT)

$[(x-32)(5/9)]\ ^{o}F = y\ ^{o}C$

### METRIC TO ENGLISH

#### LENGTH (APPROXIMATE)

1 millimeter (mm) = 0.04 inch (in)
1 centimeter (cm) = 0.4 inch (in)
1 meter (m) = 3.3 feet (ft)
1 meter (m) = 1.1 yards (yd)
1 kilometer (km) = 0.6 mile (mi)

#### AREA (APPROXIMATE)

1 square centimeter ($cm^2$) = 0.16 square inch (sq in, $in^2$)
1 square meter ($m^2$) = 1.2 square yeards (sq yd, $yd^2$)
1 square kilometer ($km^2$) = 0.4 square mile (sq mi, $mi^2$)
1 hectare (he) = 10,000 square meters ($m^2$) = 2.5 acres

#### MASS - WEIGHT (APPROXIMATE)

1 gram (gr) = 0.036 ounce (oz)
1 kilogram (kg) = 2.2 pounds (lb)
1 tonne (t) = 1,000 kilograms (kg) = 1.1 short tons

#### VOLUME (APPROXIMATE)

1 milliliters (ml) = 0.03 fluid ounce (fl oz)
1 liter (l) = 2.1 pints (pt)
1 liter (l) = 1.06 quarts (qt)
1 liter (l) = 0.26 gallon (gal)
1 cubic meter ($m^3$) = 36 cubic feet (cu ft, $ft^3$)
1 cubic meter ($m^3$) = 1.3 cubic yards (cu yd, $yd^3$)

#### TEMPERATURE (EXACT)

$[(9/5)\ y + 32]\ ^{o}C = x\ ^{o}F$

#### QUICK INCH-CENTIMETER LENGTH CONVERSION

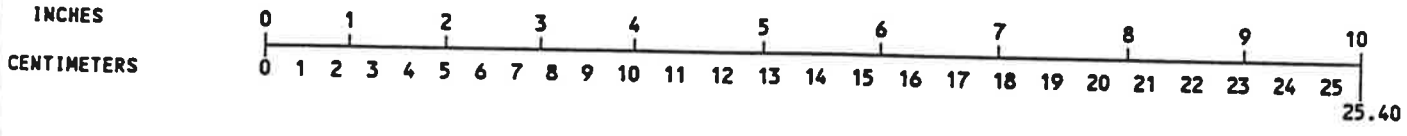


#### QUICK FAHRENHEIT-CELSIUS TEMPERATURE CONVERSION

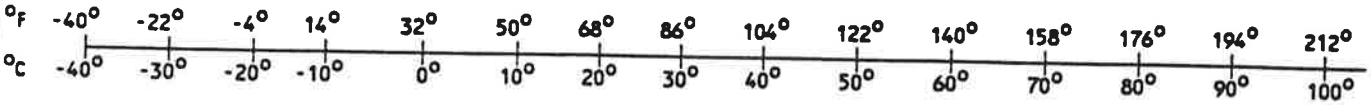


For more exact and or other conversion factors, see NBS Miscellaneous Publication 286, Units of Weights and Measures. Price $2.50. SD Catalog No. C13 10286.

## TABLE OF CONTENTS


| Section | | Page |
|---|---|---|
| 1. | OBJECTIVE | 1 |
| 2. | BACKGROUND | 1 |
| | 2.1 Gleeble Test | 1 |
| | 2.2 Class L Wheel Steel | 1 |
| | 2.3 As-received Microstructure | 2 |
| 3. | LABORATORY PROCEDURES | 2 |
| 4. | RESULTS | 3 |
| | 4.1 Macrographs | 3 |
| | 4.2 Micrographs and Quantitative Metallography | 3 |
| | 4.3 Microhardness | 4 |
| 5. | DISCUSSION | 4 |
| | 5.1 Strain Effects: Slip Line Field Theory | 4 |
| | 5.2 Temperature Effects: Recrystallization | 4 |
| | 5.3 "Ideal" Macrostructures | 5 |
| | 5.4 Summary | 5 |
| | 5.5 Hardness | 5 |
| 6. | CONCLUSIONS | 6 |
| APPENDIX A | | 8 |

## LIST OF FIGURES


| Figure | | Page |
|---|---|---|
| 1a. | Orientation and dimensions of Gleeble specimens between tungsten carbide anvils prior to deformation | 11 |
| 1b. | Appearance of the Gleeble specimen after deformation | 12 |
| 2a. | Plot of lengthwise strain and temperature versus time produced for each specimen during compression on the Gleeble | 13 |
| 2b. | The same plot as 2a expanding the region where compression occurred | 14 |
| 3. | Micrograph of sample 593-3 (deformed at 1100°F to 0.8% total strain) | 15 |
| 4. | Schematic of the plane of polish of a post-deformation specimen | 16 |
| 5. | 593-1, 1100°F, 13.6%e, B, 400x Grains of the DAR microstructure | 17 |
| 6. | 593-2, 1100°F, 4.2%e, E, 1500x SEM micrograph of UAR pearlite | 17 |
| 7. | 704-4, 1300°F, 3.2%e, all, 15x | 18 |
| 8. | 593-2, 1100°F, 4.2%e, all, 15x | 18 |
| 9. | 593-1, 1100°F, 13.6%e, all, 15x The X macrostructure | 19 |
| 10. | Schematic of Figure 9 showing the pattern revealed by etching | 19 |
| 11. | 593-1, 1100°F, 13.6%e, C, 400x Highly sheared, HS, microstructure | 20 |

## LIST OF FIGURES (continued)


| Figure | | Page |
|---|---|---|
| 12a. | 760-2, 1400°F, 12.8%e, D, 400x<br>Partially transformed, PT, microstructure | 21 |
| 12b. | 593-2, 1100°F, 4.2%e, E, 1500x<br>SEM micrograph of PT microstructure | 21 |
| 13. | 760-2, 1400°F, 12.8%e, F, 1000x<br>Equiaxed ferrite and pearlite grains<br>of the FR microstructure | 22 |
| 14. | Schematic showing the planes of maximum shear<br>strain within the specimen during compression | 23 |
| 15. | 677-3, 1250°F, 22%e, C, 165x<br>Composite micrograph of sheared grains<br>along the plane of maximum shear | 24 |
| 16. | 732-1, 1350°F, 16%e, all, 15x<br>Recrystallization initiation at specimen center<br>by PT consumption of HS microstructure | 25 |
| 17. | 732-3, 1350°F, 13.2%e, various, 400x<br>Recrystallization progression | |
| | (a) Location C of Figure 4 | 26 |
| | (b) Location B of Figure 4 | 26 |
| | (c) Location G of Figure 4 | 27 |
| | (d) Location H of Figure 4 | 27 |
| 18. | 760-3, 1400°F, 15.8%e, all, 15x<br>Recrystallization suppression of<br>specimen faces by anvil cooling | 28 |
| 19a. | 704-2, 1300°F, 10%e, all, 15x<br>Presence of HS and DAR grains among<br>PT and FR grains of the S macrostructure | 29 |
| 19b. | Schematic of Figure 19a distinguishing<br>the areas of the different microstructures | 29 |

## LIST OF FIGURES (continued)


| Figure | | Page |
|---|---|---|
| 20. | 649-1, 1200°F, 19.2%e, I, 200x | 30 |
| 21. | 704-3, 1300°F, 14.0%e, all, 15x | 30 |
| 22. | Plot of microstructure at the specimen center for all samples at corresponding strain values and temperatures | 31 |

## LIST OF TABLES


| Table | | Page |
|---|---|---|
| 1. | The testing parameters for each Gleeble specimen | 9 |
| 2. | Volume percent ferrite and ASTM grain size ± the 95% confidence interval or standard deviation with the percent relative accuracy for each microstructure | 10 |
| 3. | Knoop microhardness numbers in $kgf/mm^2$ measured for each grain | 10 |

## 1. OBJECTIVE

Characterize the microstructural development of Class L steel wheels under heavy braking by means of thermomechanical testing.

## 2. BACKGROUND

### 2.1 Gleeble Test

The test involves hot compression of 22 specimens to various target strain values at temperatures above and below the eutectoid transition temperature (1340°F) on a Gleeble 1500. Variations of test temperature and monotonic plastic strain are utilized to simulate service conditions. The tests were conducted by Dr. R. Parthasarathy at the Oregon Graduate Institute of Science and Technology, Beaverton, Oregon, as part of a research grant from the Federal Railroad Administration. Specimens are rectangular prisms with 5x10x20 mm dimensions (Figure 1a). Samples are resistance-heated. Type K thermocouples, percussion-welded to the 5x20 mm surface, monitor and control the temperature. Hydraulic compression produces plane deformation through the 5 mm thickness between 5 mm-wide tungsten carbide anvils held in stainless steel jaws (Figures 1a and b). A linear voltage differential transducer (LVDT) measures the lengthwise displacements over the 5 mm gauge length. A strain rate of 100 mm/mm/second is maintained. The high rate of strain requires blocks to arrest crosshead movement at the desired target displacement value. Data obtained during testing are plots of temperature and lengthwise strain versus time (Figures 2a and b). The actual thickness achieved is measured after testing and is used to calculate average permanent strain (Table 1).

### 2.2 Class L Wheel Steel

Different classes, serving as guidelines for intended service conditions, designate the wheel's steel composition, heat treatment, and final hardness. Class L steel was developed for light wheel loads on high-speed trains with more severe braking conditions than what is expected of the other classes. This steel contains not more than 0.47 weight percent (w/o) C, between 0.60 and 0.85 w/o Mn, less than 0.05 w/o each of S and P and more than 0.15 w/o Si. Its heat treatment consists of a post-forming reheat to approximately 1600°F and a water quench of the rim only. Again reheating the wheels and furnace cooling to below 300°F tempers the quenched rim. A single Brinell measurement using a 3000 kgf load and 10 mm ball on the front rim face at a distance of more than 4.8 mm from the tread must yield a hardness number between 197 and 277 kgf/mm$^2$ (214 and 302 kgf/mm$^2$ on the Knoop scale).

## 2.3 As-received Microstructure

Because of the post-forming heat, quench, and temper to which the rim is subjected, Class L steel wheels' microstructure depends upon the position within the wheel from which the specimen is taken. Gleeble samples were machined from an in-service wheel.

The undeformed, as-received (UAR) microstructure is shown in Figure 3. It is assumed to accurately represent the microstructure present in all specimens prior to deformation, despite its origins. Specimen 593-3 was heated to 1100°F and strained 0.8 percent. However, the micrograph location was far removed from any deformation (area A of Figure 4). Characteristic of hypoeutectic steels, this microstructure contains the micro-constituents ferrite and pearlite. Ferrite grains, the blocky-shaped white areas of all optical microstructures presented, are proeutectoid grain boundary allotriomorphs (GBA) which nucleate at intersections between austenite grains upon cooling. The constituents also precipitated as Widmanstatten plates, spiny protrusions of a GBA (see Figure 5). The pearlite of Figure 3, the dark gray areas, may be subdivided into colonies. Figure 6 shows the lamellae at a magnification of 1500x. In scanning electron microscope (SEM) micrographs, ferrite appears as black areas and iron carbide as white.

# 3. LABORATORY PROCEDURES

Specimens are mounted in Fina-Met thermosetting polymer powder using Struers' Prestopress-3. Initial rough grinding of the 5x20 mm faces (Figure 1b) is unnecessary, requiring only fine grinding following the standard 240-320-400-600-grit sequence on a Leco VP-50 Vari/Pol automatic polisher. Fine polishing is performed by hand on a napless wheel with 1.0, 0.3, and 0.05 micron alumina. A two percent nitric acid in alcohol (nital) etchant is used. Macrographs of samples under an Excell ultraviolet light are taken at 15x with a Nikon SMZ-10 stereo microscope. Micrographs of select samples are taken at magnifications between 165 and 1000x on Olympus Vanox or Nikon Optiphot microscopes.

Quantitative metallography of micrographs yields the grain size and percentage of each phase present. Appendix A contains relevant definitions, equations, and procedures.

Knoop microhardness values of the microstructures in each sample are measured using a Leco DM-400 microhardness tester with a 300-gram load. Finally, sample 593-2 is gold-coated to enhance surface conduction and viewed under the Cambridge Instruments Stereoscan 250Mk3 SEM at 1500x.

## 4. RESULTS

### 4.1 Macrographs

Etching reveals three distinct patterns discernible to the naked eye. Macrographs of the patterns, or macrostructures, are presented in Figures 7 through 10. In Figure 7, no pattern appears before or after deformation. This is the as-received (A) macrostructure. In Figure 8, material stressed by the anvils is lighter than uncompressed material of the specimen's ends. This is the stressed (S) macrostructure. In Figure 9, the pattern appears as a cross connecting opposite anvil edges. This is the X macrostructure. Although it did not photograph well, it is schematically represented in Figure 10.

Polishing displaces the plane of polish to an estimated depth of 0.2 to 0.3 mm beneath the original surface. Further grinding of samples 593-1, 621-1, 649-1 and -2, 704-2, and 760-2 to approximately 1.7 mm reveals the same macrostructures.

### 4.2 Micrographs and Quantitative Metallography

The material possesses the UAR microstructure of Figure 3 prior to testing. Its effective grain size is 8.95 with a relative accuracy (RA) of 9.5%. The range of grain sizes, given by the standard deviation, is 8.65 to 9.4. The ferrite volume fraction ($V\alpha$) is 30.6% with a 95% confidence interval ($CI_{95\%}$) of ±2.6% and a RA of 8.6%. The balance, for all microstructures, is pearlite (Table 2). Also, the ferrite GBA surround pearlite grains.

After testing, etching resolves four distinct microstructures in all samples. These microstructures are presented at 400x in Figures 5, 11, 12a, and at 1000x in Figure 13. Microstructural discrimination is accomplished by determination of the grain size, shape, and hardness, the volume fraction of each phase, and its orientation with respect to others.

In some samples, the region stressed by the anvils has grains similar to the UAR microstructure. These grains constitute the deformed as-received microstructure (DAR). The similarity between DAR and UAR microstructures is the grain size. Figure 5 shows the difference: $V\alpha$ decreases to 20.3%, $CI_{95\%}$ = ±4.7%, RA = 23.1% and, the pearlite-enveloping nature of the ferrite is more distinguished than in the UAR microstructures.

The highly sheared microstructure (HS) is shown in Figure 11. The grains appear to have the size of the UAR and DAR grains although severe elongation renders grain size determination impossible. The ferrite still surrounds the pearlite. Also, $V\alpha$ decreases to a low value of 15.5%, $CI_{95\%}$ = ±3.2%, RA = 20.4%.

In striking contrast with the other microstructures, the partially transformed microstructure (PT, Figure 12a) shows a breakdown of pearlite (Figure 12b). Instead of ferrite GBA surrounding pearlite, small grains of both ferrite and pearlite exist, bringing the grain size down to 11.85 + 0.35 - 0.40, RA = 8.2%. Unlike DAR and HS, $V\alpha$ in the PT microstructure increases over the UAR value to 48.9%, $CI_{95\%} = \pm 3.9\%$, RA = 8.0%.

The fully recrystallized microstructure (FR) significantly decreases the grain size with respect to UAR, shrinking to an effective size of 13.1 + 0.35 - 0.40, RA = 11.1% (Figure 11). Ferrite grains are equiaxed, do not surround pearlite, and comprise 62.1% ($CI_{95\%} = \pm 1.9\%$, RA = 3.0%) of the volume.

### 4.3 Microhardness

Testing ranks the grains in descending order of hardness to be HS, FR, DAR, UAR, and PT. Knoop microhardness numbers are given in Table 3.

## 5. DISCUSSION

### 5.1 Strain Effects: Slip Line Field Theory

For plane strain conditions, slip line field theory predicts, for the sample-anvil geometry tested (Figure 1a), planes of maximum shear stress produced in the sample to run diagonally through the body from each anvil edge to the opposite anvil edge (Figure 14). This partially explains the hot compression test results.

Maximum shear stress planes delineate regions of heavy plastic deformation. Therefore, the appearance of HS grains at anvil edges is expected with either UAR or DAR grains appearing elsewhere. Figure 15 illustrates this and the continuation of strained grains toward the specimen center. The HS grains manifest the X macrostructure on a macroscopic level. Thus, applying sufficient strain produces the X macrostructure with HS, DAR, and UAR microstructures from a specimen initially containing A and UAR structures.

### 5.2 Temperature Effects: Recrystallization

PT and FR microstructures develop from the HS microstructure. HS grains contain much stored energy, a result of heavy plastic deformation, and consequently act as primary recrystallization sites. Recrystallization occurs in these regions, but initiates at specimen centers. Figure 16 shows specimen center PT microstructure development. Reference to Figures 17a through d reveals the absence of recrystallization in HS grains, yet FR grains appear at the specimen's center and PT grains appear between these and the surface. Therefore, grains of advancing PT and FR microstructures consume the strained matrix, ultimately leading to the S macrostructure of Figure 8.

Recrystallization initiation at specimen centers is odd. Recrystallization ease generally increases with strain and temperature. Grains near anvil edges are strained much more than the center. Therefore, recrystallization is expected to start at the edge and move toward the center. Anvil cooling of the specimen face may suppress this. In Figure 18, extensive recrystallization occurred throughout, except for the faces in contact with anvils.

### 5.3 "Ideal" Macrostructures

Ideal macrostructures (Figures 7 through 10) are symmetrical and contain one macrostructure. All macrostructures contain UAR grains at the specimen ends. The A macrostructure contains UAR and DAR grains. The X macrostructure is devoid of PT and FR grains while the S macrostructure is HS-grain-free. Complications to these basic relationships exist and result in a mixture of two macrostructures.

The first complication results from the extent of recrystallization. Cooling the sample shortly after the onset of recrystallization incompletely consumes the HS microstructure. This was noted for Figures 16 and 17 and gives compelling evidence that the HS grains transform to PT and then FR grains. The same phenomena are also seen in sample 704-2 where all four microstructures exist (Figure 19a and b).

Tantalum strips between specimen and anvil reduce friction during compression. Figure 20 shows they also induce recrystallization in DAR grains. The specimen otherwise contained only the HS, DAR, and UAR microstructures expected of the X macrostructure.

The final complication depends on the grips and anvils. Uneven compression bends the sample; one side strains more than the other. This causes each side to recrystallize differently. This is evident to a slight degree in Figures 19a and b and undoubtedly in Figure 21.

### 5.4 Summary

The observations made here are summarized in the recrystallization map of Figure 22. The expected result: increasing the test temperature, for a given strain level, generally causes recrystallization. Unexpectedly, however, increasing the strain at a given temperature may reduce recrystallization. Specifically, recrystallization occurred extensively at 1100°F with only 4.2% strain (sample 593-2) while at 1150°F, a strain of 4.6% (sample 621-3) had no effect on the microstructure and at 1200°F, a strain of 6.6% (sample 649-2) leads to recrystallization, but to a much lesser degree. Thus, it is possible that anvil-cooling does not solely suppress HS grain recrystallization. Rather, the high strain level of these grains, may slow recrystallization.

### 5.5 Hardness

All average Knoop hardness numbers of the microstructures fall within the allowed specifications (Table 3). Of the microstructures, only the FR grains' hardness is scattered enough to approach the upper bound of 302 kgf/mm$^2$. The variation between microstructures is caused

by the amount of strain (high dislocation density), grain size and volume fraction of iron carbide (pearlite), all being impediments to dislocation motion. Thus, the hardness should increase from UAR to DAR and HS since the strain increases and $V\alpha$ decreases. The dip in hardness of the PT grains must be caused by the higher $V\alpha$ and the release of strain energy upon initializing transformation since the grain size shrank. Also, the increase in FR grain hardness must be a result of the small grain size despite the increase in $V\alpha$ and the release of all strain energy.

## 6. CONCLUSIONS

Hot compression of Class L steel on a Gleeble 1500 yields:

- Transformation to four microstructures: deformed as-received (DAR), highly sheared (HS), partially transformed (PT), and fully recrystallized (FR).
- Ferrite and pearlite as micro-constituents for all microstructures.
- Microstructure-dependent micro-constituent volume fractions.
- Decreasing microhardness of the microstructures from HS to FR, DAR, UAR, and PT.
- An ordering of the microstructures by strain levels and temperature into three different macrostructures: as-received (A), stressed (S), and crossed (X).
- Recrystallization of HS grains with increasing temperature.
- Possible recrystallization suppression of HS grains upon increasing strain levels.

## REPORTS IN THIS SERIES


1. O. Orringer, D.E. Gray, and R.J. McCown, *Evaluation of Immediate Actions Taken to Deal with Cracking Problems Observed in Wheels of Rail Commuter Cars*, Volpe National Transportation Systems Center, Cambridge, MA, and Federal Railroad Administration, Washington, DC, report no. FRA/ORD-93/15, July 1993.

2. C. Stuart and S. Yu, *Thermal Measurements of Commuter Rail Wheels Under Revenue Service Conditions*, Ensco, Inc., Springfield, VA, report no. FRA/ORD-93/19, September 1993.

3. Y.H. Tang, J.E. Gordon, A.B. Perlman, and O. Orringer, *Finite Element Models, Validation, and Results for Wheel Temperature and Elastic Thermal Stress Distributions*, Volpe National Transportation Systems Center, Cambridge, MA, report no. FRA/ORD-93/17, September 1993.

4. Y.H. Tang, J.E. Gordon, O. Orringer, and A.B. Perlman, *Stress Reconstruction Analysis of Wheel Saw Cut Tests and Evaluation of Reconstruction Procedure*, Volpe National Transportation Systems Center, Cambridge, MA, report no. FRA/ORD-93/18, September 1993.

## APPENDIX A

Values reported are averages, X, of sampled data, $X_i$. The scatter of the data is given by the standard deviation:

$$SD = \sqrt{[(n-1)^{-1}\sum(X-X_i)^2]}$$

where n is the number of times the property is measured. The calculated average's accuracy with respect to the actual property value is given by the 95% confidence interval:

$$CI_{95\%} = Z_n SD/\sqrt{(n-1)}$$

where $Z_n$ is a factor ranging between 2 and 3 and is dependent upon n. The percent relative accuracy of the averaged measured property is simply:

$$\%RA = 100CI_{95\%}/X$$

In the determination of the grain size, ASTM Standard Test Method E 112-88 was used. Specifically, the effective grain size (so termed because it determines the grain size for both phases simultaneously by treating them as a single phase) technique was followed since the microstructure of the steel contained two phases. The average number of intercepts per mm and corresponding standard deviation was calculated from the summation of grain boundary intercepts of all individual test lines from all fields. The effective grain size was determined using this average while the ± range was determined by adding and subtracting the standard deviation from the average and redetermining the grain size. Consequently, the ± range did not center around the average.

To find the volume percent of ferrite present, ASTM Standard Test Method E 562-89 was used. A 49-point grid was laid over micrographs with magnifications of 200, 500, and 1000x, depending on the grain size. The percent of points per field was averaged over many fields to directly give the volume fraction.

Table 1. The testing parameters for each Gleeble specimen.

| SPECIMEN NUMBER | TEMPERATURE °F | TARGET STRAIN | % STRAIN ACHIEVED |
|---|---|---|---|
| 760-1 | 1400 | 20 | 20.2 |
| 760-2 | 1400 | 10 | 14.0 |
| 760-3 | 1400 | 5 | 16.2 |
| 760-4 | 1400 | 1 | 4.8 |
| 732-1 | 1350 | 20 | 17.8 |
| 732-3 | 1350 | 5 | 13.2 |
| 704-1 | 1300 | 20 | 22.5 |
| 704-2 | 1300 | 10 | 11.2 |
| 704-3 | 1300 | 5 | 15.1 |
| 704-4 | 1300 | 1 | 2.8 |
| 677-1 | 1250 | 20 | 22.0 |
| 677-3 | 1250 | 5 | 21.2 |
| 649-1 | 1200 | 20 | 21.2 |
| 649-2 | 1200 | 10 | 6.1 |
| 649-3 | 1200 | 5 | 13.1 |
| 649-4 | 1200 | 1 | 1.6 |
| 621-1 | 1150 | 20 | 15.6 |
| 621-3 | 1150 | 5 | 4.8 |
| 593-1 | 1100 | 20 | 15.6 |
| 593-2 | 1100 | 10 | 5.4 |
| 593-3 | 1100 | 5 | 3.4 |
| 593-4 | 1100 | 1 | 21.8 |

Table 2. Volume percent ferrite and ASTM grain size ± the 95% confidence interval or standard deviation with the percent relative accuracy for each microstructure. "Same" and "Elongated" refer to comparisons with UAR.

| | UAR | DAR | HS | PT | FR |
|---|---|---|---|---|---|
| Sample | 593-3 | 593-1 | 593-1 | 760-2 | 760-2 |
| Vα<br>$\pm CI_{95\%}$<br>%RA | 30.6<br>±2.6<br>8.6 | 20.3<br>±4.7<br>23.1 | 15.5<br>±3.2<br>20.4 | 48.9<br>±3.9<br>8.0 | 62.1<br>±1.9<br>3.0 |
| G<br>±SD<br>%RA | 8.95<br>+0.45-0.30<br>9.5 | Same | Elongated | 11.85<br>+0.35-0.40<br>8.2 | 13.10<br>+0.35-0.40<br>11.1 |

Table 3. Knoop microhardness numbers in kgf/mm$^2$ measured for each grain. "Location" refers to the specimen region of Figure 4 from which data was collected.

| | UAR | DAR | HS | PT | FR |
|---|---|---|---|---|---|
| Location | A | B, H, J | C | G, H, J | H |
| Hardness<br>$\pm CI_{95\%}$<br>%RA | 257.2<br>±7.5<br>2.9 | 268.6<br>±5.4<br>2.0 | 276.0<br>±11.2<br>4.1 | 250.5<br>±8.8<br>3.5 | 273.8<br>±25.5<br>9.3 |

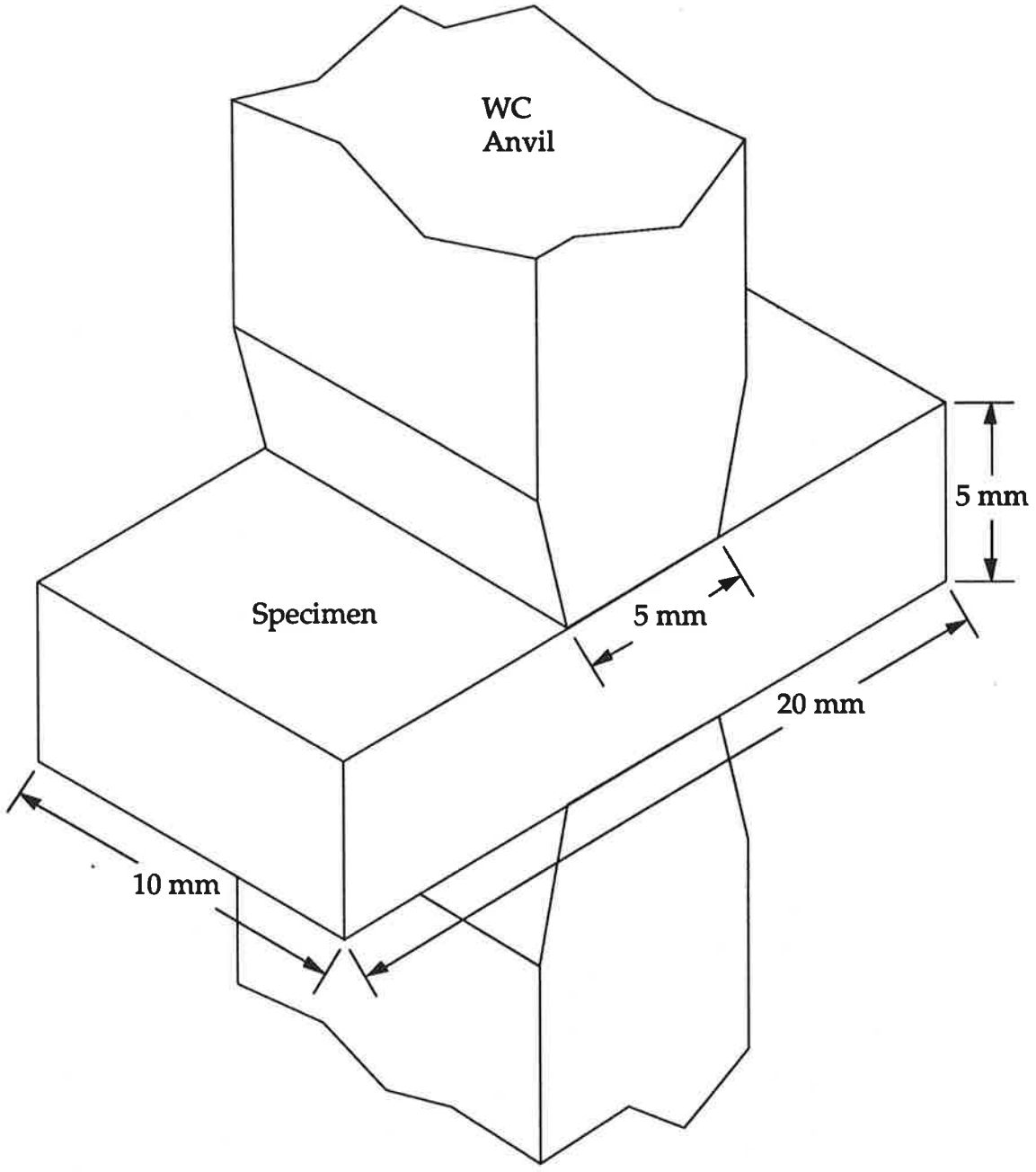


Figure 1a. Orientation and dimensions of Gleeble specimens between tungsten carbide anvils prior to deformation.

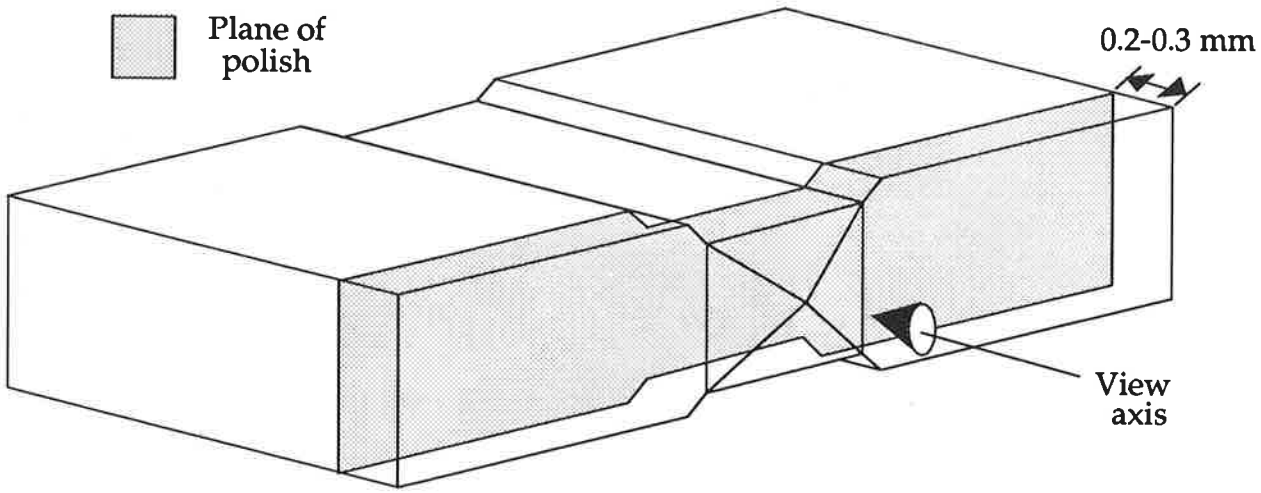


Figure 1b. Appearance of the Gleeble specimen after deformation.

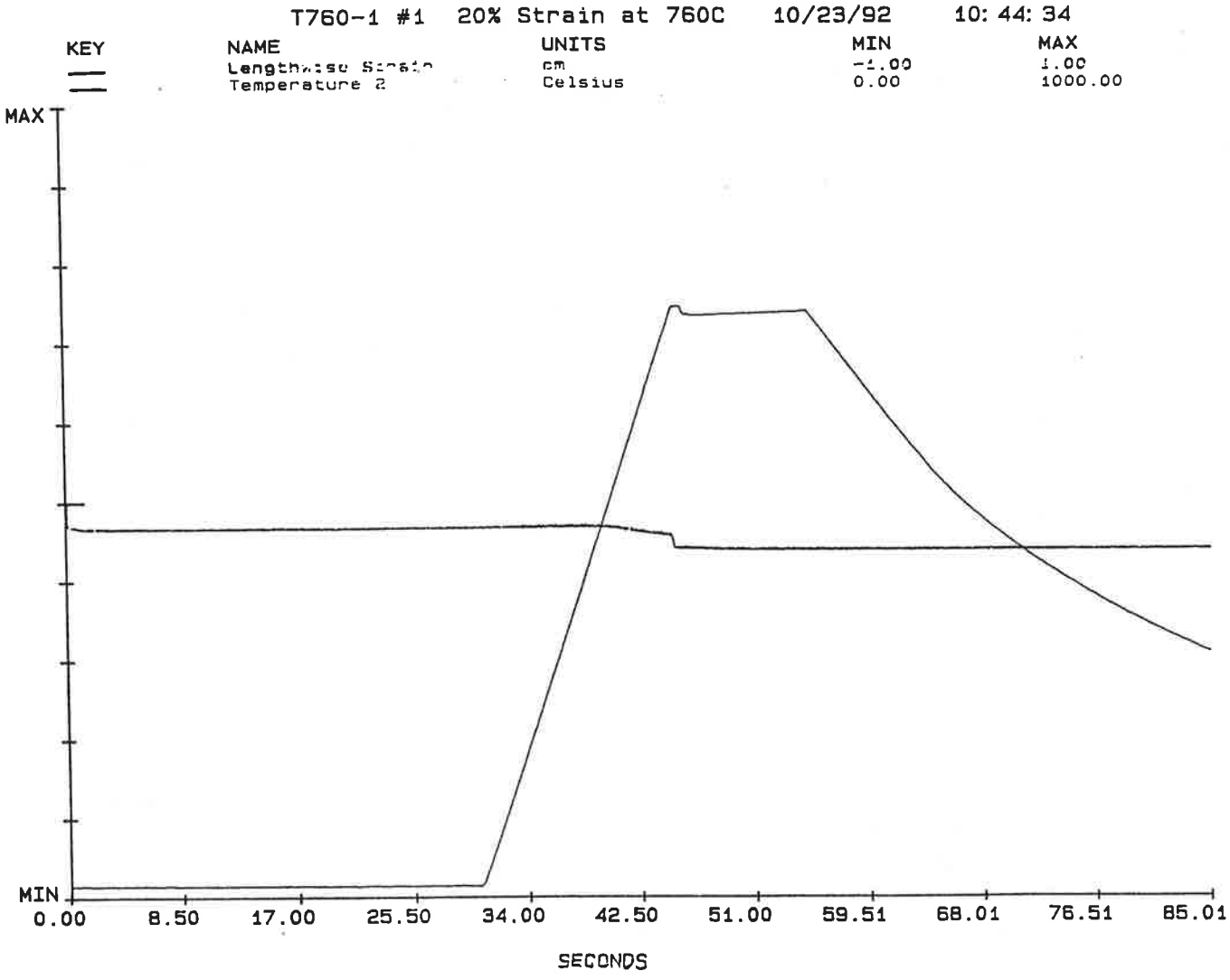


Figure 2a. Plot of lengthwise strain and temperature versus time produced for each specimen during compression on the Gleeble.

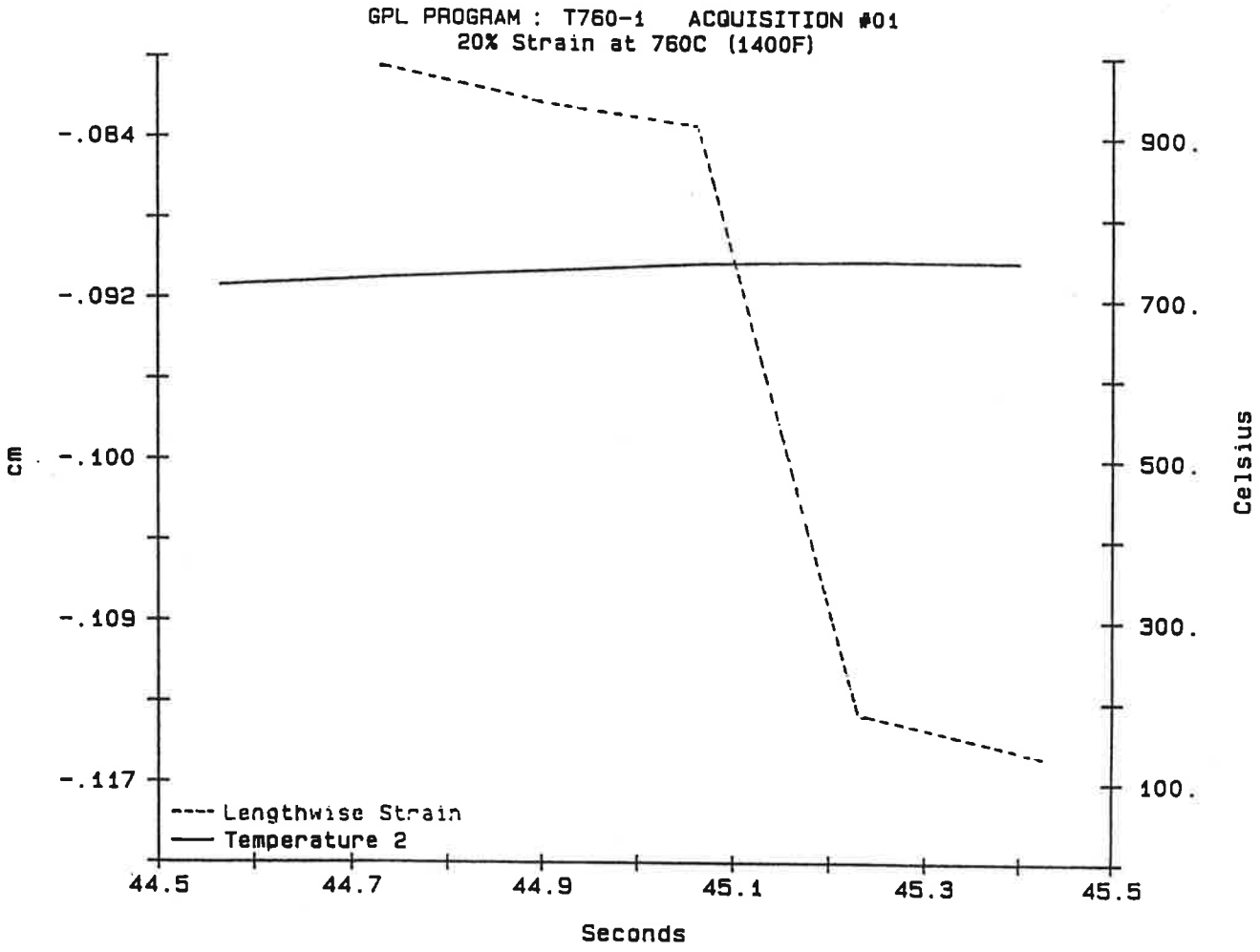


Figure 2b. The same plot as 2a expanding the region where compression occurred.

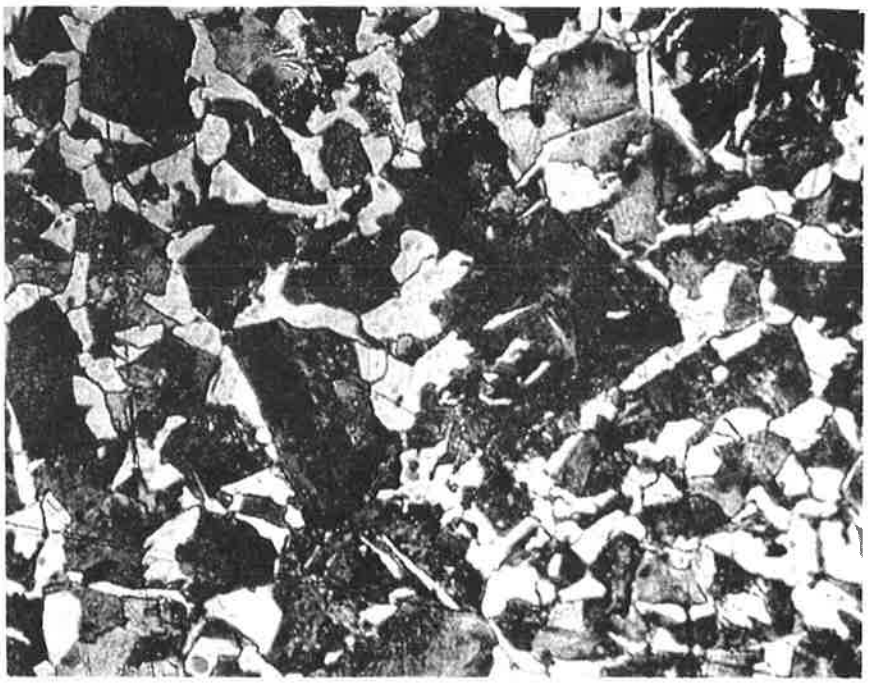

Figure 3. Micrograph of sample 593-3 (deformed at 1100°F to 0.8% total strain). This micrograph is taken from undeformed, as-received (UAR) area A of Figure 4 at a magnification of 400x (abbreviated format: 593-3, 1100°F, 0.8%e, A, 400x). The UAR microstructure prior to deformation. White blocks are proeutectoid ferrite GBA. Darker areas are pearlite grains.

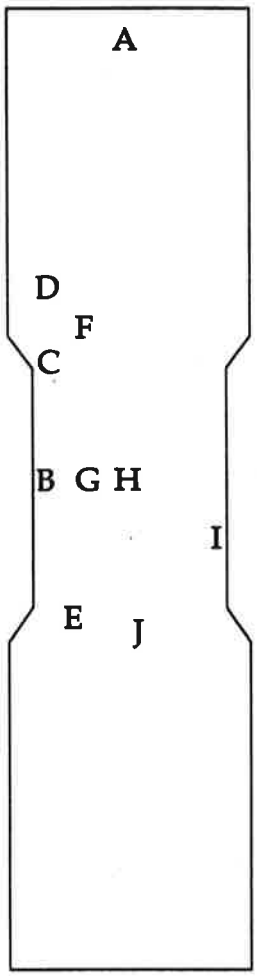


Figure 4. Schematic of the plane of polish of a post-deformation specimen. The letters denote cited photomicrograph locations.

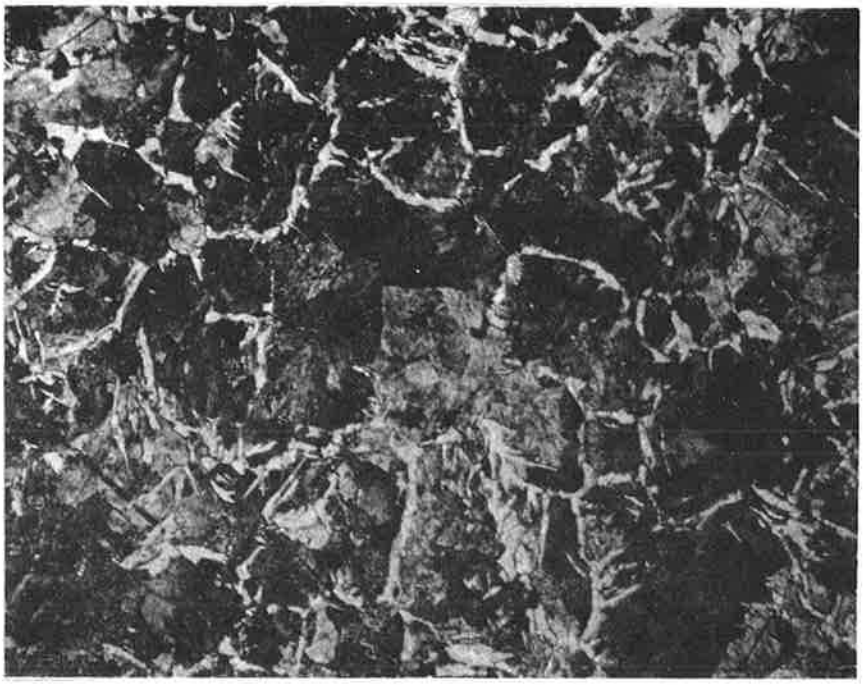

Figure 5. 593-1, 1100°F, 13.6%e, B, 400x
Grains of the DAR microstructure. Some ferrite GBA have Widmanstatten plates.

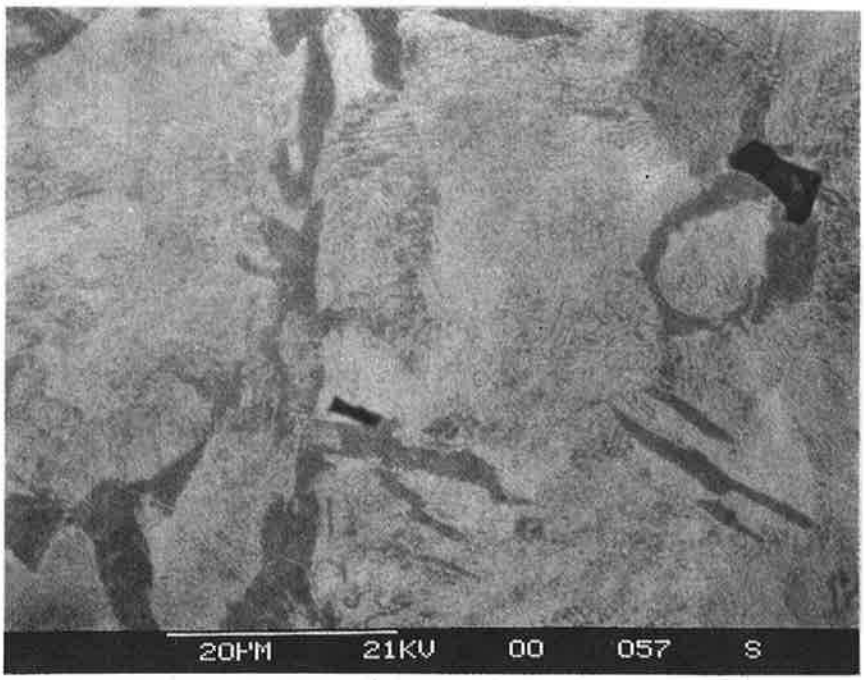


Figure 6. 593-2, 1100°F, 4.2%e, E, 1500x
SEM micrograph of UAR pearlite. The large black areas are ferrite GBA. The fine structure is caused by lamellar colonies of ferrite and iron carbide.

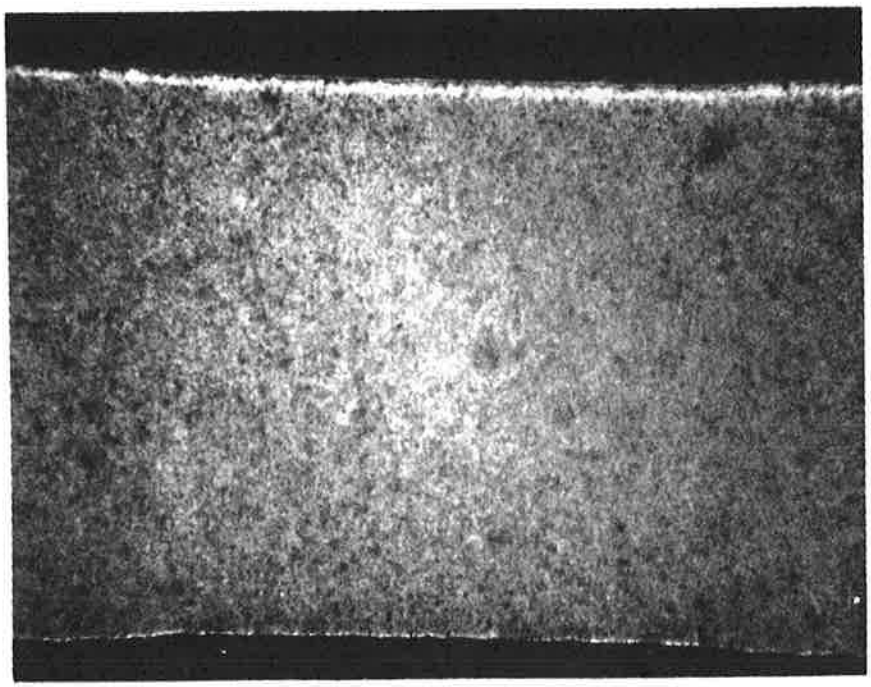

Figure 7. 704-4, 1300°F, 3.2%e, all, 15x
The patternless A macrostructure appears the same before and after deformation.

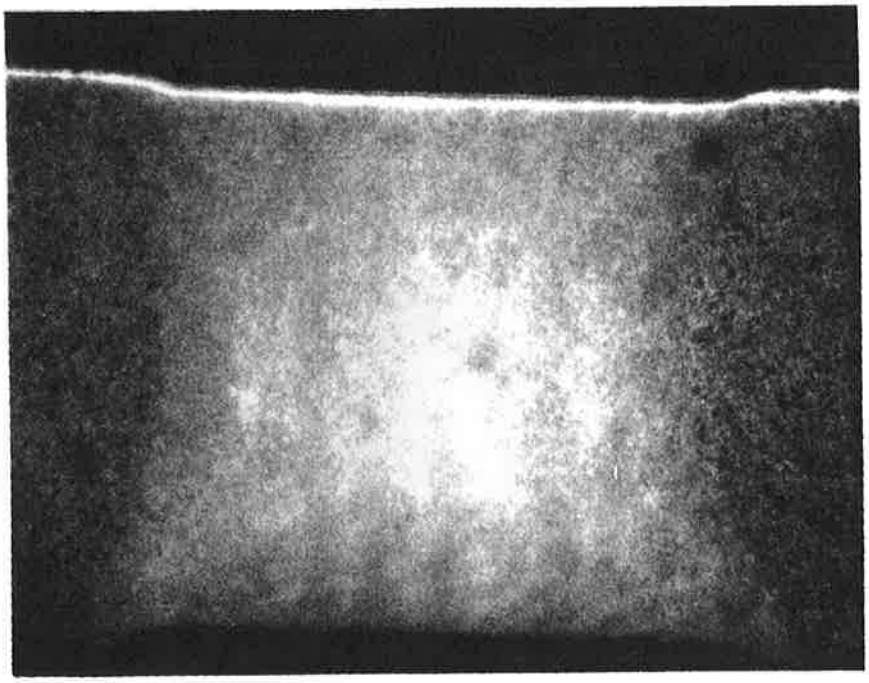

Figure 8. 593-2, 1100°F, 4.2%e, all, 15x
The stressed region between anvils appears lighter in the S macrostructure.

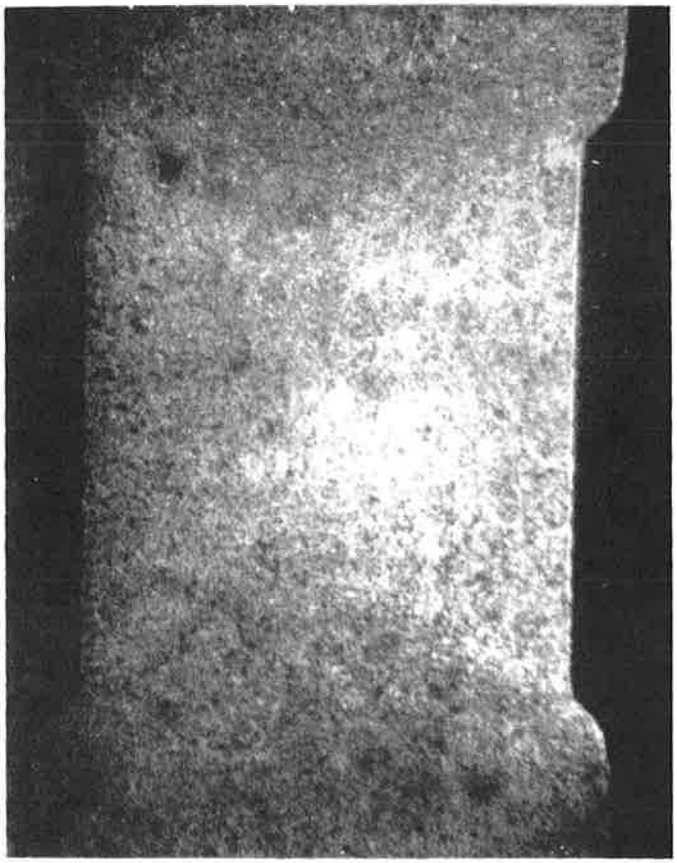

Figure 9. 593-1, 1100°F, 13.6%e, all, 15x
The X macrostructure.

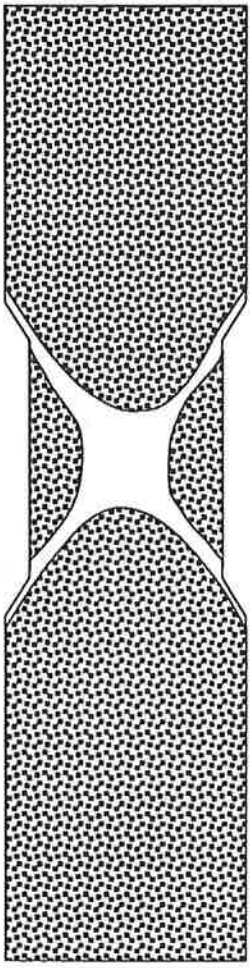

Figure 10. Schematic of Figure 9 showing the pattern revealed by etching.

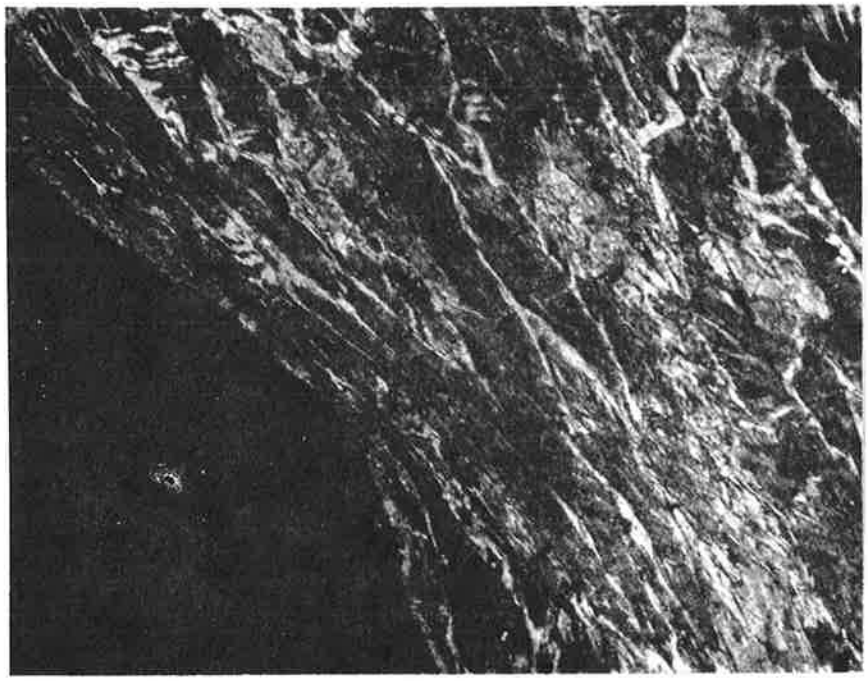

Figure 11. 593-1, 1100°F, 13.6%e, C, 400x. Highly sheared, HS, microstructure.

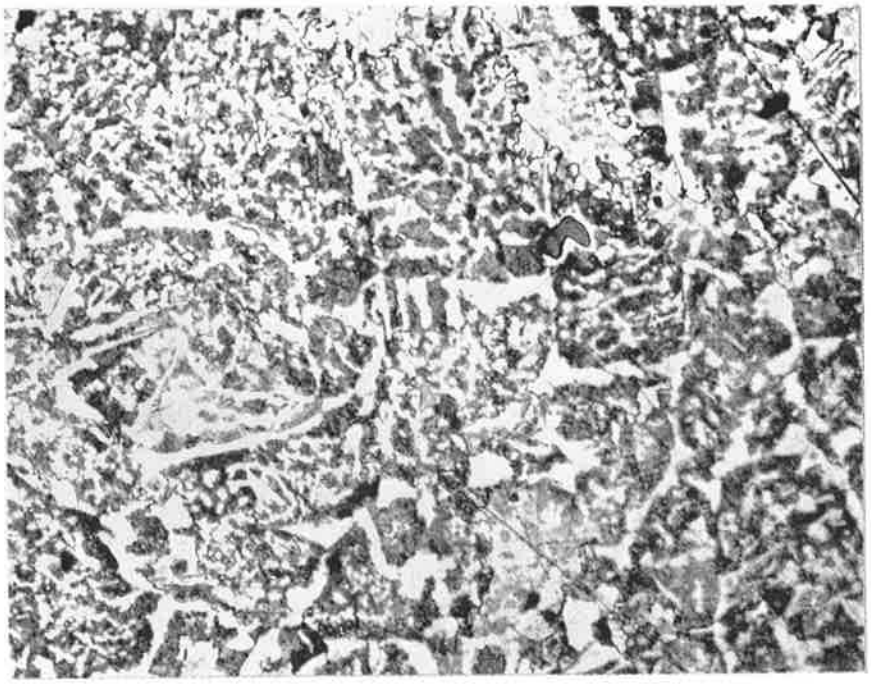

Figure 12a. 760-2, 1400°F, 12.8%e, D, 400x. Partially transformed, PT, microstructure.

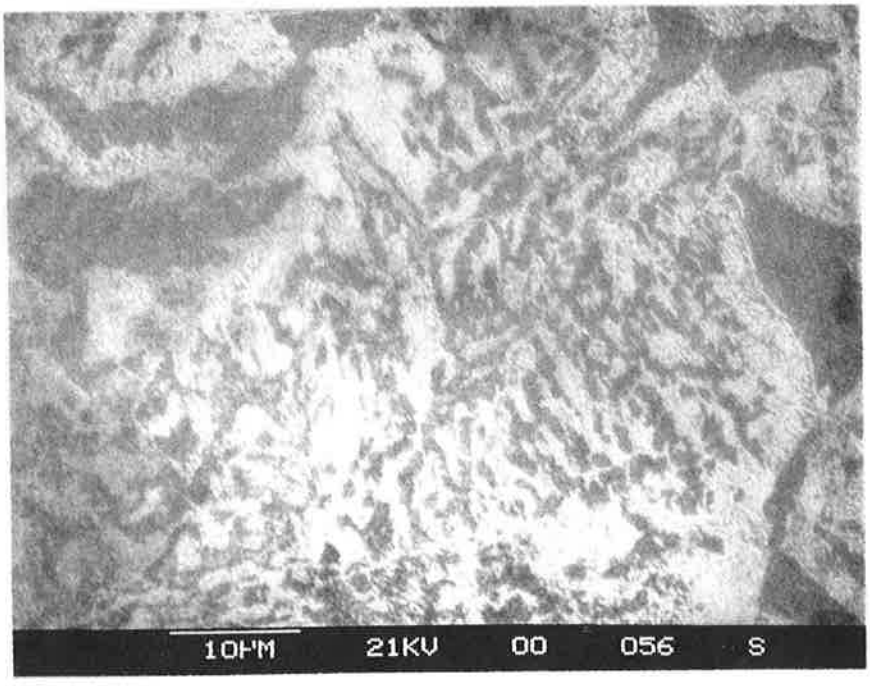


Figure 12b. 593-2, 1100°F, 4.2%e, E, 1500x
SEM micrograph of PT microstructure. Broken down pearlite exists as small grains of pearlite and ferrite. The large dark areas are ferrite GBA.

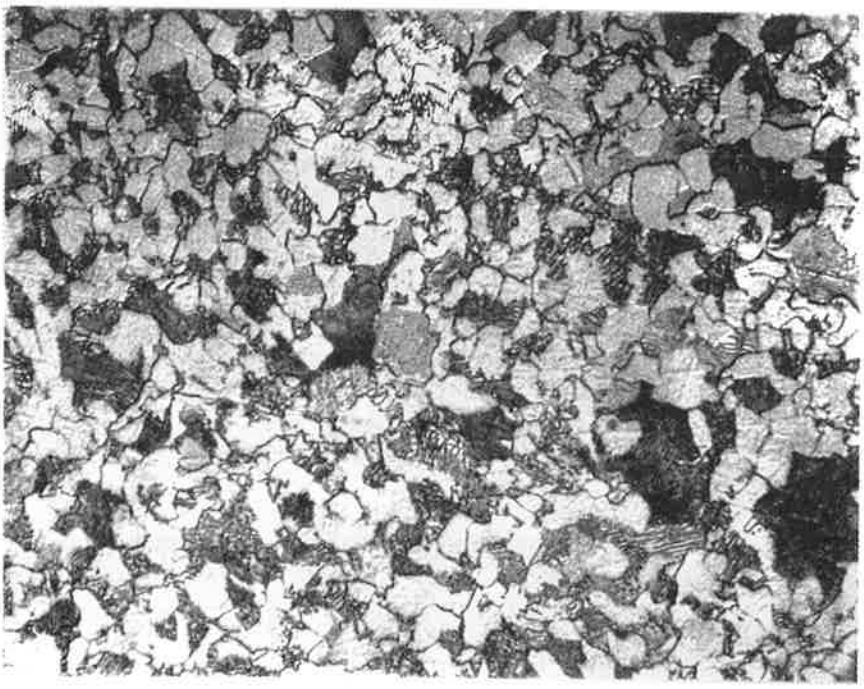

Figure 13. 760-2, 1400°F, 12.8%e, F, 1000x
Equiaxed ferrite and pearlite grains of the FR microstructure.

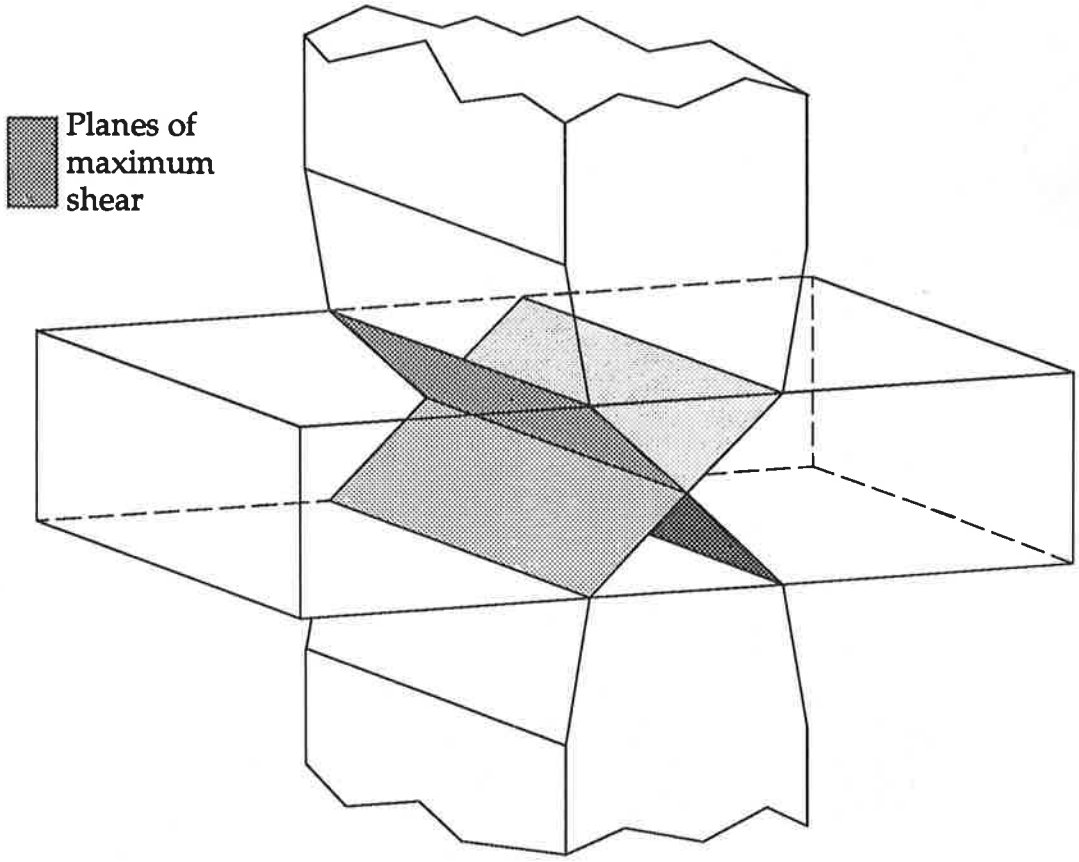


Figure 14. Schematic showing the planes of maximum shear strain within the specimen during compression.

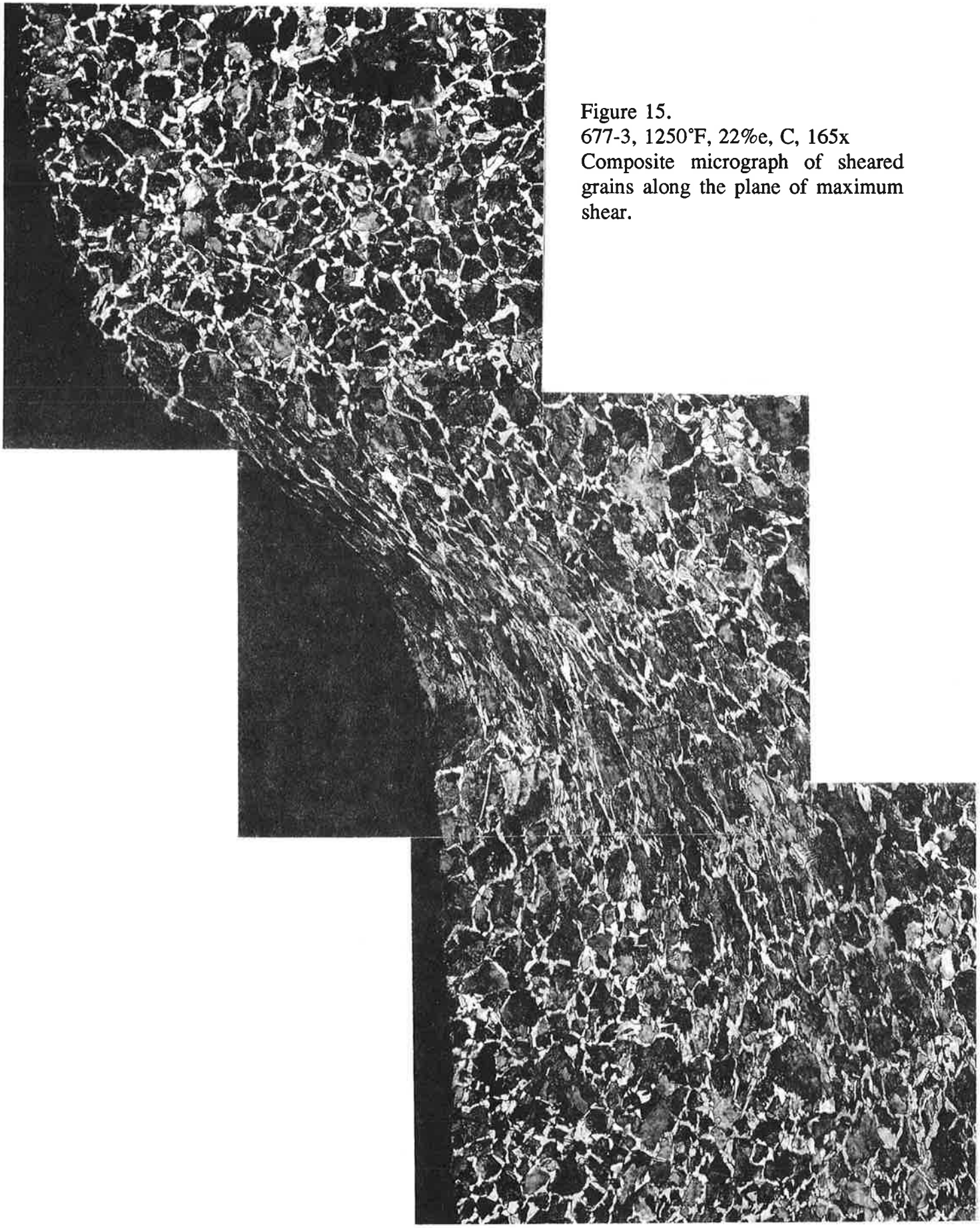

Figure 15.
677-3, 1250°F, 22%e, C, 165x
Composite micrograph of sheared grains along the plane of maximum shear.

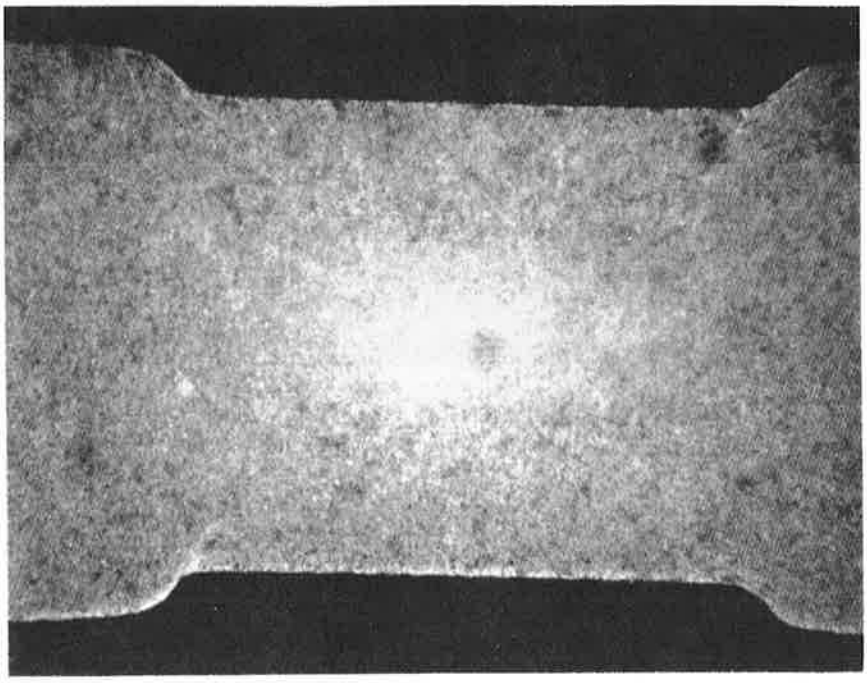

Figure 16. 732-1, 1350°F, 16%e, all, 15x
Recrystallization initiation at specimen center by PT consumption of HS microstructure. The macrostructure is a mixture of X and S.

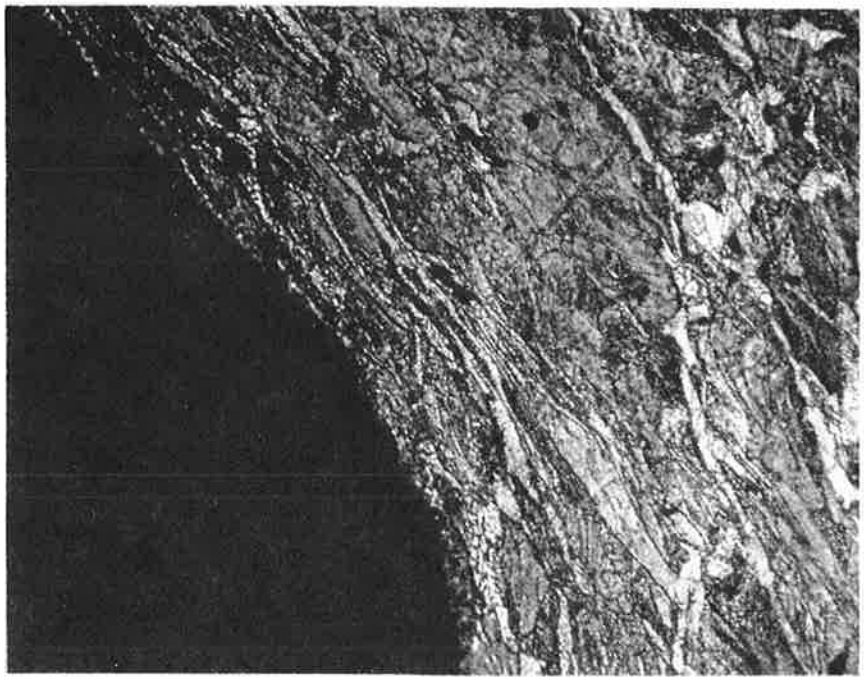

Figure 17a. The HS grains at the anvil edge (location C of Figure 4) remain unrecrystallized despite the high amounts of local strain.

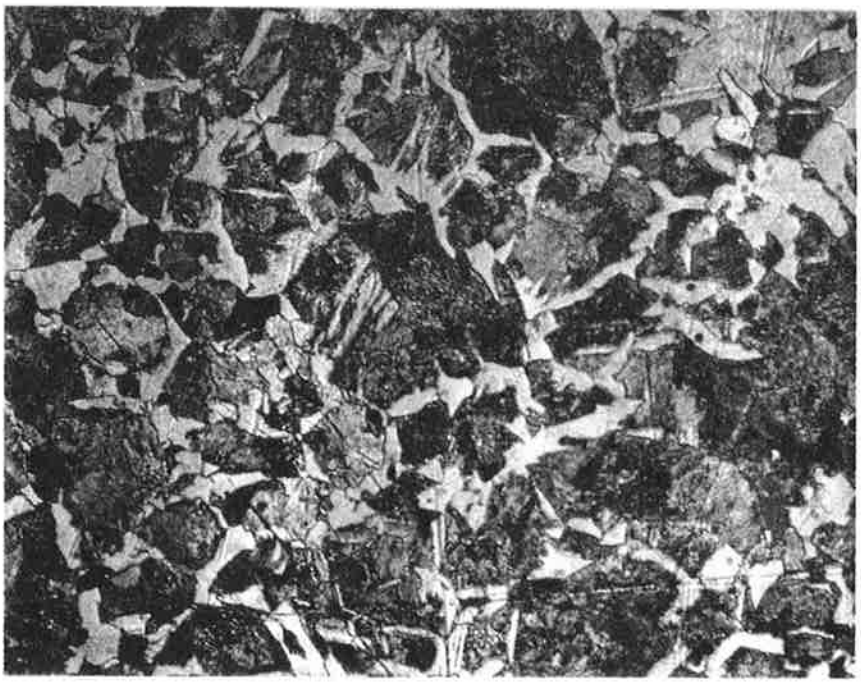

Figure 17b. The DAR grains of the anvil face (location B of Figure 4) also remain unrecrystallized.

Figure 17. 732-3, 1350°F, 13.2%e, various, 400x. Recrystallization progression.

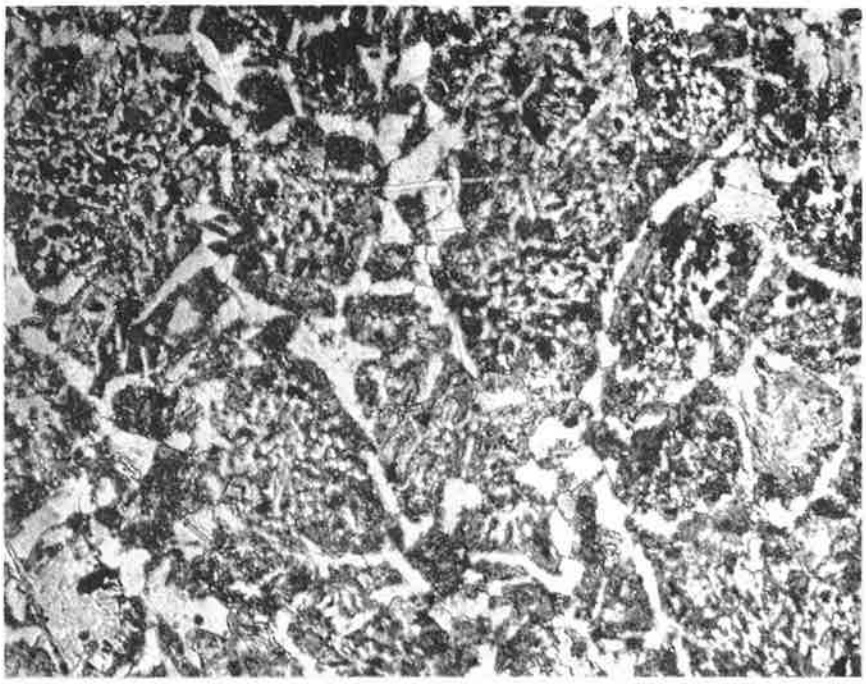

Figure 17c. PT grains appear midway between the anvil face and the center of the specimen (location G of Figure 4) indicating that recrystallization initiates at the center and proceeds outward.

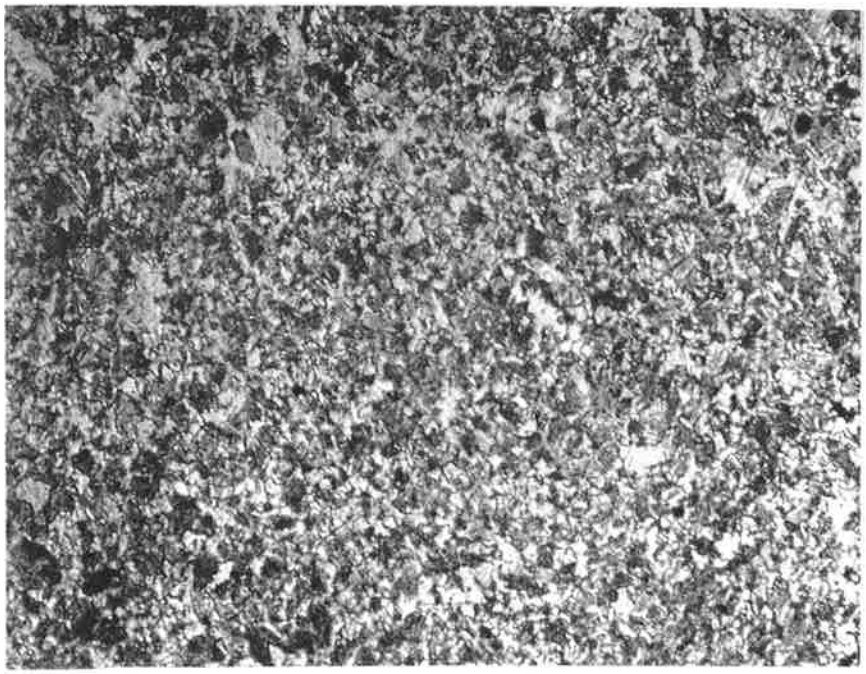

Figure 17d. The presence of FR grains at the center (location H of Figure 4) confirms the center to be the recrystallization initiation point.

Figure 17. 732-3, 1350°F, 13.2%e, various, 400x. Recrystallization progression (continued).

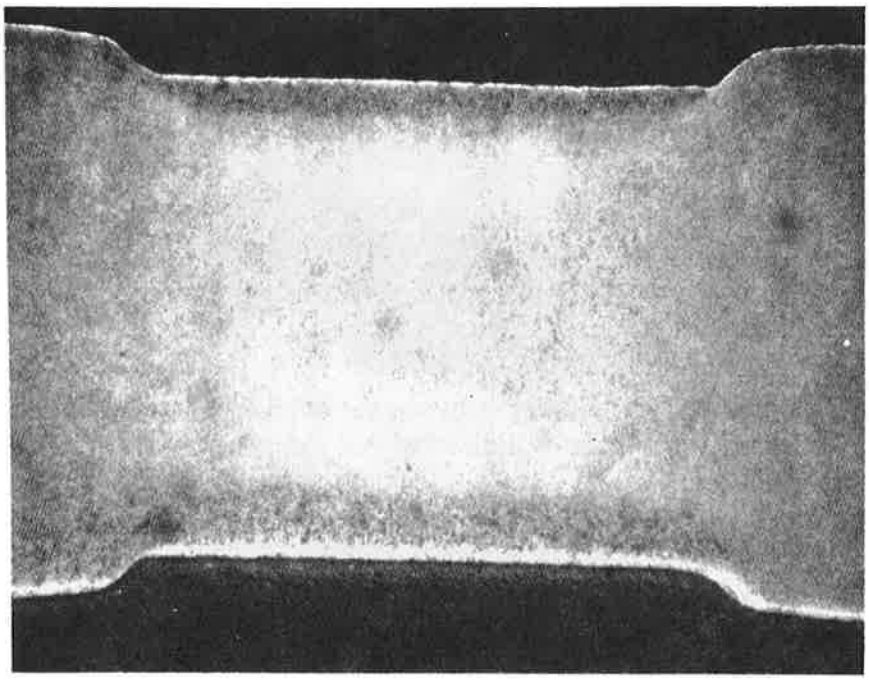

Figure 18. 760-3, 1400°F, 15.8%e, all, 15x
Recrystallization suppression of specimen faces by anvil cooling.

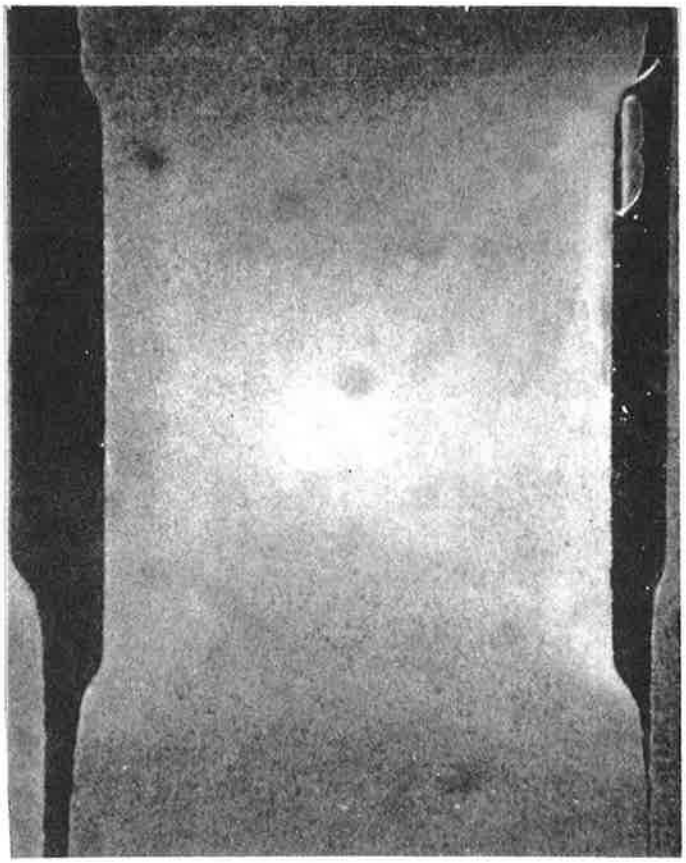

Figure 19a. 704-2, 1300°F, 10%e, all, 15x
Presence of HS and DAR grains among PT and FR grains of the S macrostructure.

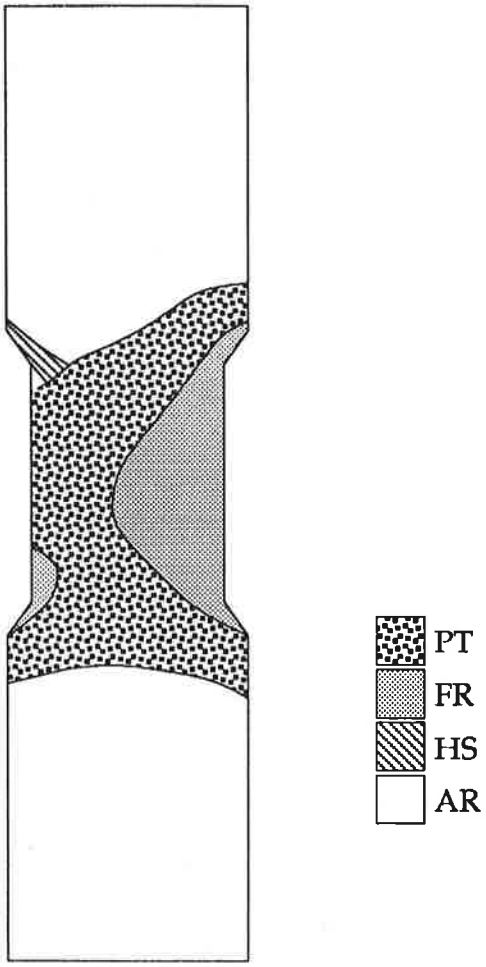


Figure 19b. Schematic of Figure 19a distinguishing the areas of the different microstructures.

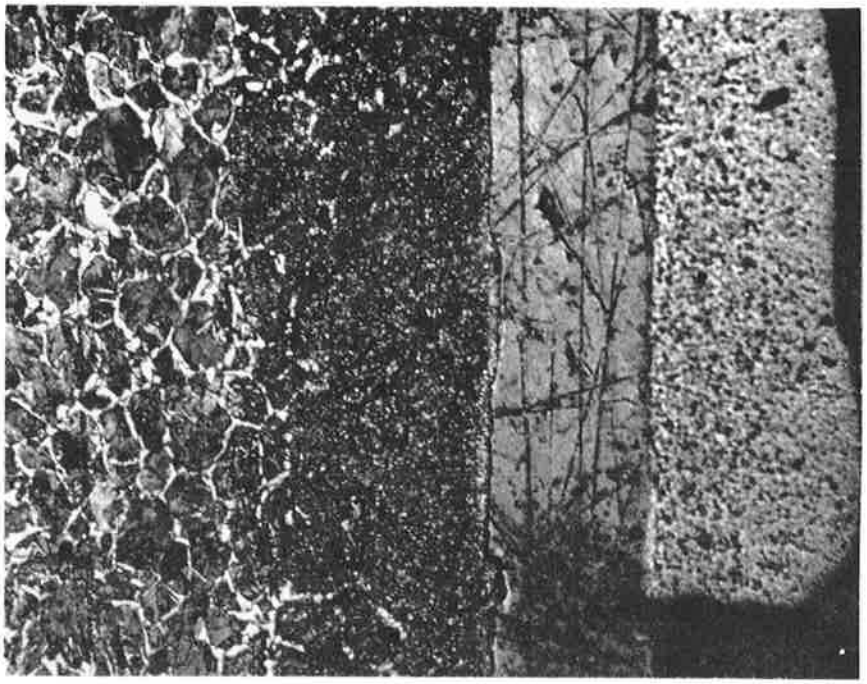

Figure 20. 649-1, 1200°F, 19.2%e, I, 200x
The tantalum sheet used to prevent the anvils from sticking to the specimens and to reduce friction during deformation is seen to cause recrystallization in the DAR microstructure.

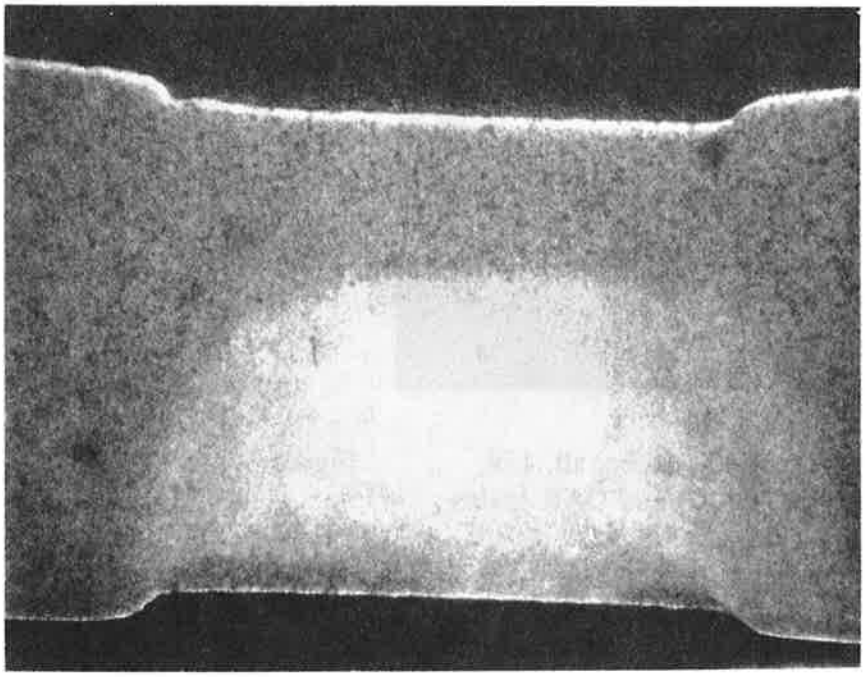

Figure 21. 704-3, 1300°F, 14.0%e, all, 15x
Bending of the specimen during testing distributes strain unevenly and causes asymmetrical macrostructures to form and varying recrystallization.

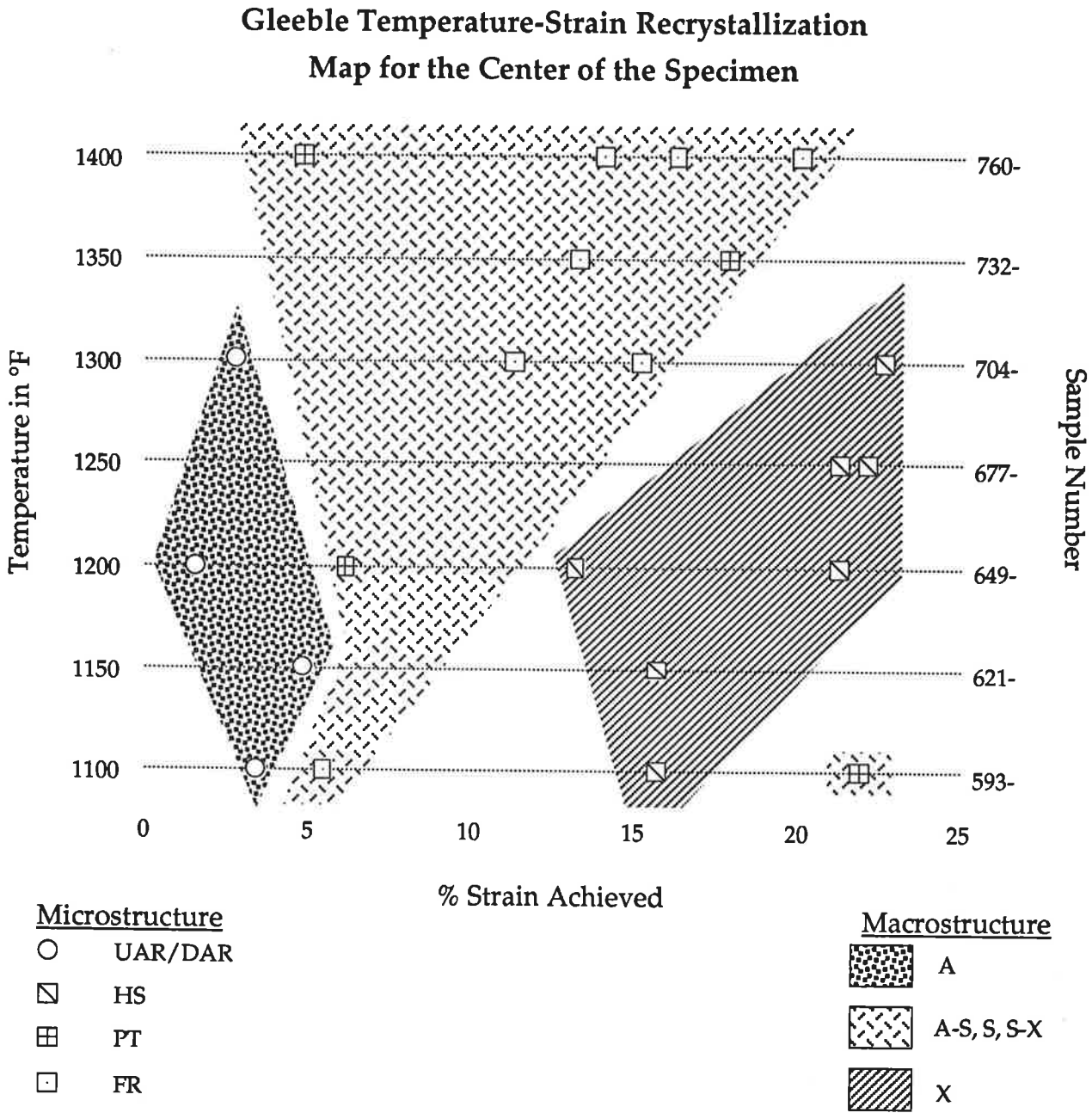


Figure 22. Plot of microstructure at the specimen center for all samples at corresponding strain values and temperatures. The macrostructures fall on the map according to strain regimes. Note that the S macrostructure regime also contains asymmetrical and mixed macrostructures while the A and X regimes do not.